# Diameter-Dependent Optical Constants of Gold Mesoparticles Electrodeposited on Aluminum Films Containing Copper

**Dmitri A. Brevnov*,† and Corey Bungay‡**

*Department of Chemical and Nuclear Engineering, Center for Micro-Engineered Materials, The University of New Mexico, Albuquerque, New Mexico 87131, and J.A. Woollam Co. Inc., Lincoln, Nebraska 68508*

*Received: March 7, 2005; In Final Form: May 23, 2005*

Electrodeposition of gold mesoparticles on anodized and chemically etched aluminum/copper films deposited on silicon wafers proceeds by instantaneous nucleation and with no diffusion limitations. Both of these phenomena favor the formation of relatively monodispersed gold particles. Under the reported electrodeposition conditions, the relative standard deviation of the particle diameter is 25%. The particle coverage is $7 \times 10^8$ particles $cm^{-2}$. The mean particle diameter varies as a function of electrodeposition time in the range of 40−80 nm. Optical constants of gold mesoparticles are resolved by spectroscopic ellipsometry. A two-layer optical model is constructed to determine both extinction coefficients and refractive indexes of gold mesoparticles as a function of the mean particle diameter. The absorption peak, associated with surface plasmons, is modeled with two Lorentz oscillators. Absorption peak maximums shift from 610 to 675 nm as the mean particle diameter increases from 42 to 74 nm. Electrodeposition of gold particles on technologically relevant substrates, such as aluminum/copper films, is expected to increase the utility of gold particles and facilitate their incorporation in nanostructured materials and a variety of electronic and optical devices.

## Introduction

Solution-based methods to synthesize metallic, nano- (1−10 nm) and meso- (10 nm to 1 $\mu$m) particles, especially of gold and silver, have been known for decades.[1−3] These particles are considered as building units for nanostructured materials, due to their optical, electrical, and catalytic properties.[1−5] For deposition of metallic particles on a surface, the majority of reported procedures advocate the employment of a wet-chemistry method involving a reducing agent and a high oxidation state metal precursor.[6] Subsequently, free-standing metallic particles prepared in solution are collected and transferred to a desired substrate. By using this strategy, particles can be synthesized in large quantities and with a narrow distribution of particle diameters, with the latter property being the primary advantage. Regardless of wide utilization of this approach in research laboratories, two factors limit its practical usefulness. First, transferring may result in poor adhesion and, consequently, no electrical connection of metallic particles to the underlying support. Second, controlling the particle coverage and aggregation may be problematic. Therefore, to increase the utility of metallic particles, it is important to develop deposition methods, which produce strongly adhesive and particulate films with a narrow distribution of particle diameters. The fabrication of these films on technologically relevant substrates would allow us to fully exploit optical and electrical properties of metallic particles and facilitate their incorporation in functional materials. Subsequently, these materials can be utilized for fabrication of waveguides, solar cells, information storage devices, chemical/biochemical sensors, and a number of other optical and electronic devices.[7−9]

Among a variety of methods employed for deposition of metallic particles, electrodeposition stands out as an inexpensive and versatile technique.[10−22] Electrodeposition of metals on conductive substrates covered with a thin dielectric layer is suitable for fabrication of particulate films because electrodeposition usually occurs by the three-dimensional island growth (Volmer−Weber) mechanism.[10−12] This mechanism has been reported for electrodeposition of metallic particles, including Au,[13] Cu on Si;[14,15] Cu on TaN;[16,17] Ag[18] and Pt[19] on atomically smooth graphite basal plane surfaces; Ag on Si;[20] Ag and Au on Si;[21] and Pb and Cu on Si.[22] Electrodeposition of metallic particles has been shown to follow models for either instantaneous or progressive nucleation.[10−12] For both models, the growth of particles can proceed under kinetic, diffusion, or mixed control. As in solution-based methods, a narrow distribution of particle diameters can be achieved only if nucleation is instantaneous and, as a result, separated in time from the growth of particles. Moreover, it is mandatory that, during electrodeposition, diffusion zones among growing particles do not overlap.[12] Under these two conditions, the particle coverage is mainly controlled by the applied potential and the thickness of the dielectric layer.[23] The mean particle diameter is controlled by electrodeposition time, concentration of a reduced species, and temperature of deposition solution.[10−12] In addition to being used for deposition of metallic particles, electrodeposition in combination with chemical methods has been employed for fabrication of particles composed of metal oxides and semiconductor materials.[21]

Since metallic particles are frequently prepared in solution, their extinction coefficients are readily determined by UV−vis spectrophotometry. The optical properties of metallic particles vary slightly as a function of particle diameter.[25−27] According to Kreibig and Vollmer, the dielectric function of metallic particles with a diameter larger than about 10−20 nm has values of bulk metal.[25] Accordingly the size dependence of gold mesoparticles optical response is "an *extrinsic cluster-size effect* governed only by the dimension of the particle with respect to

* Address correspondence to this author. E-mail: dbrevnov@unm.edu.
† The University of New Mexico.
‡ J.A. Woollam Co. Inc.

10.1021/jp0511707 CCC: $30.25 
Published on Web 07/08/2005

the wavelength of the light".[25] The spectra of gold mesoparticles are characterized by a strong absorption band due to surface plasmons.[1,5−6,9] For gold particles, the position and bandwidth of the absorption band depend on the mean particle diameter, the particle shape, the distribution of particle diameters, and the dielectric constant of the surrounding medium.[9,25−28] For gold particles in an aqueous solution with mean diameters of 9, 15, 22, 48, and 99 nm, maximums of surface plasmon bands were observed at 517, 520, 521, 533, and 575 nm, respectively.[29] For silver particles fabricated on transparent substrates, extinction maximums were tuned over a wide range of wavelengths by controlling the particle size, height, and shape and by encapsulating these particles in a dielectric medium.[30]

In contrast to straightforward determination of extinction coefficients of metallic particles in solution, the optical constants of particulate films on reflective substrates can be resolved only by either UV−visible reflectance spectroscopy or spectroscopic ellipsometry (SE).[31−36] The latter technique is inherently more sensitive than the former. Better sensitivity results from the fact that SE variables ($\psi$ and $\Delta$), which are defined by the ratio of Fresnel reflection coefficients for s- and p- polarized light, are measured as the ratio of two signals. However, SE has been rarely applied for determination of optical constants of metallic particles mainly due to difficulties with the deposition of monodispersed particles.[6,32] In addition, interpretation of ellipsometric spectra may be problematic because of uncertainties with modeling of the background spectrum of a bare substrate. The great majority of SE spectra have been obtained with metallic particles deposited on bare or modified silicon wafers, a substrate which has been thoroughly investigated by SE.[34] The absorption band due to surface plasmons of gold particles is typically modeled by using a Lorentz oscillator, with the peak position around 550 nm.[35,36] For gold particles embedded in dielectric media (e.g. $SiO_2$), effective medium approximation (EMA) theories have been applied to extract information about the nanocomposite films.[37−39] Due to the scarcity of SE data for particulate films of noble metals electrodeposited on aluminum substrates, there is an incentive to apply SE for determination of optical constants of gold particles.

Technologically relevant aluminum/copper films can be made amenable for subsequent electrodeposition of gold particles by anodization followed by chemical etching of aluminum oxide.[40] Electrodeposition on anodized and etched aluminum/copper films covered with a thin layer of aluminum oxide proceeds by the Volmer−Weber mechanism because the surface free energy of gold ($\sim$1.3 J/m$^2$) is higher than that of aluminum oxide ($\sim$0.64 J/m$^2$). Under galvanostatic conditions ($\sim$1 mA/cm$^2$) electrodeposition of approximately 1-$\mu$m gold particles occurs by instantaneous nucleation and under kinetic control.[40] Both of these phenomena favored the formation of monodispersed particles. Gold particles were electrodeposited with a coverage of $10^5$−$10^7$ particles cm$^{-2}$. In this case, the gold particle coverage was too low and the mean particle diameter was too large for characterization of gold particles by SE.

The objectives of this project were 2-fold. The first was to implement a fast and facile procedure for activation of aluminum/copper films and electrodeposition of gold mesoparticles with mean particle diameters less than 100 nm and coverage higher than that reported previously.[40] Electrodeposition of gold mesoparticles with a relatively narrow distribution of diameters allowed for employment of SE to probe the optical constants of gold mesoparticles. Under controlled electrodeposition conditions, the particle coverage could be held constant and the mean particle diameter varied. The second objective was to employ SE to investigate the position of a surface plasmon band as a function of the mean particle diameter. While the former was obtained from the analysis of SE spectra, the latter was determined from the examination of scanning electron micrographs.

## Experimental Section

Silicon wafers with an intermediate 0.6-$\mu$m layer of $SiO_2$ and 3-$\mu$m metallic layer (99.5 wt % aluminum and 0.5 wt % copper) were fabricated and processed as described previously.[40] Gold electrodeposition on anodized and etched aluminum/copper films was carried out at room temperature (22 °C), in 1.0 M $Na_2SO_3$ (pH 8),[41] with 20 mM $Na_3Au(SO_3)_2$ (Technic Inc. Oromerse Part B gold plating solution). Electrodeposition was performed with an IM6-e impedance measurement unit (Zahner) by applying a potential step from an open-circuit potential (OCP) to −3.95 V vs a Ag/AgCl electrode and under anaerobic conditions. Current transients were normalized to the electrode geometric area of 1.4 cm$^2$. The surface morphology of deposited gold particles was evaluated with a Hitachi (S-5200) scanning electron microscope (SEM) operated at 5 kV. Histograms of particle diameters were obtained with Spirit software. Single angle (70.0°) SE experiments and data analysis were performed with a M-44 ellipsometer (J. A. Woollam Co., Inc.) and WVASE32 software. Forty-four pairs of $\psi$ and $\Delta$ were collected over a wavelength range from 418 to 753 nm. The geometric area probed in SE measurements was approximately 0.5 cm$^2$. The background spectrum ($\psi$ and $\Delta$) for the optically thick anodized and etched aluminum/copper film (without gold particles) was fit to a model consisting of a substrate and a 50-nm thick Bruggeman EMA layer. The EMA layer, which approximates scallops formed on the surface as a result of anodization and chemical etching, was modeled as a 50%/50% mixture of substrate optical constants and void ($n = 1$, $k = 0$). The thickness of 50 nm was chosen because the depth of scallops was estimated to be about 50 nm. Optical constants of the anodized and etched aluminum/copper film (refractive index, $n$, and extinction coefficient, $k$) were obtained by performing a wavelength-by-wavelength fit of $\psi$ and $\Delta$ to the one layer model. Thus, the optical constants were allowed to vary independently at each wavelength. The substrate optical constants had to be measured before depositing the gold particles because they were different from optical constants of both aluminum (incorporated in the software database) and pristine aluminum/copper substrates (not subject to anodization and etching).

## Results and Discussion

Figure 1 shows the current transient acquired upon application of a potential step for 0.05 s from OCP (0.01 s) to −3.95 V (0.06 s). The electrochemical cell time constant was estimated to be 0.32 ms as the product of the uncompensated resistance (40 Ω) and capacitance of the barrier aluminum oxide layer ($\sim$8.0 $\mu$F).[40] Therefore, the charging current decayed to zero in about 1.6 ms (5 times the cell time constant), as indicated by two arrows (Figure 1). Figure 1 demonstrates that the cathodic current, attributed to the irreversible reduction of $Au(SO_3)_2^{3-}$, reached a value of −43 mA/cm$^2$ and then stayed constant as a function of time. This observation indicates that electrodeposition of gold is not under diffusion control. The increasing absolute magnitude of the cathodic current is due to the increasing surface area of gold particles during the course of electrodeposition.[10−12] Due to its high absolute magnitude ($\sim$60 mA), the cathodic current is likely to be controlled by

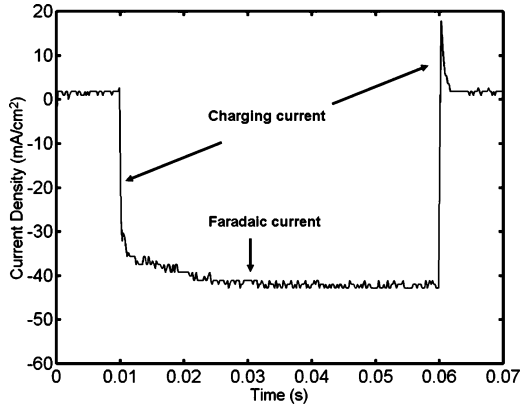


**Figure 1.** A current transient acquired upon application of a potential step from OCP to −3.95 V vs Ag/AgCl. The deposition solution was 20 mM $Na_3Au(SO_3)_2$ and 1.0 M $Na_2SO_3$.

the ohmic resistance of the electrochemical cell (40 Ω). Proton and residual oxygen reduction might also contribute to the cathodic current. Regardless of some uncertainty with the origin of the rate-limiting process, no diffusion limitation (no decrease in the absolute magnitude of the cathodic current even at very negative potentials) was observed during potential steps applied for less than 0.05 s. Therefore, diffusion zones formed around individual gold particles were unlikely to overlap during electrodeposition. Both the instantaneous nucleation and the absence of diffusion limitations favored the formation of gold particles with a relatively narrow distribution of particle diameters.

To fabricate gold particles with variable diameters, electrodeposition experiments were performed with the same applied potential of −3.95 V and variable deposition times. Panels a−c in Figure 2 show SEM micrographs collected after electrodeposition of gold particles for 0.03, 0.04, and 0.05 s, respectively. The black pseudohexagonal cells with white edges represent shallow scallops formed on the surface as a result of anodization and subsequent chemical etching. Whereas anodization generates two distinct layers of barrier and porous aluminum oxides, etching completely dissolves the porous layer and partially dissolves the layer of barrier aluminum oxide.[40] Upon completion of chemical etching, the thickness of the barrier aluminum oxide is approximately 1.5 nm.[42] As previously suggested, a combination of anodization and etching results in copper enrichment in and/or underneath the layer of barrier aluminum oxide.[40,43−45] As a consequence, electrodeposition on anodized and etched aluminum/copper films becomes possible. The analysis of Figure 2 suggests that electrodeposition proceeds via the formation of gold particles randomly located on the surface (no long term order) and with a particle coverage of approximately $7 \times 10^8$ particles $cm^{-2}$. By employing a more negative potential, a 2 orders of magnitude higher coverage than previously reported[40] was achieved in this project. For kinetically controlled electrodeposition, both the cathodic current and nucleation density increase exponentially with the applied overpotential.[10] The particle coverage varied from sample to sample by approximately 15% despite the same applied potential of −3.95 V. These variations were attributed to slight variations in the capacitance (thickness) of barrier aluminum oxide. Nucleation density is known to exponentially decrease with the thickness of a dielectric layer covering a conductive substrate.[23]

The particle diameters can be estimated by two alternative ways. The first method assumes that electrodeposited particles are spherical, their gravimetric density is equal to the bulk density of gold, and the faradaic efficiency during electrodeposition is 100%. For a one-electron reaction, the mean particle diameter, $D$ (m), is related to the faradaic charge density, $Q$ ($mC/cm^2$), by eq 1.

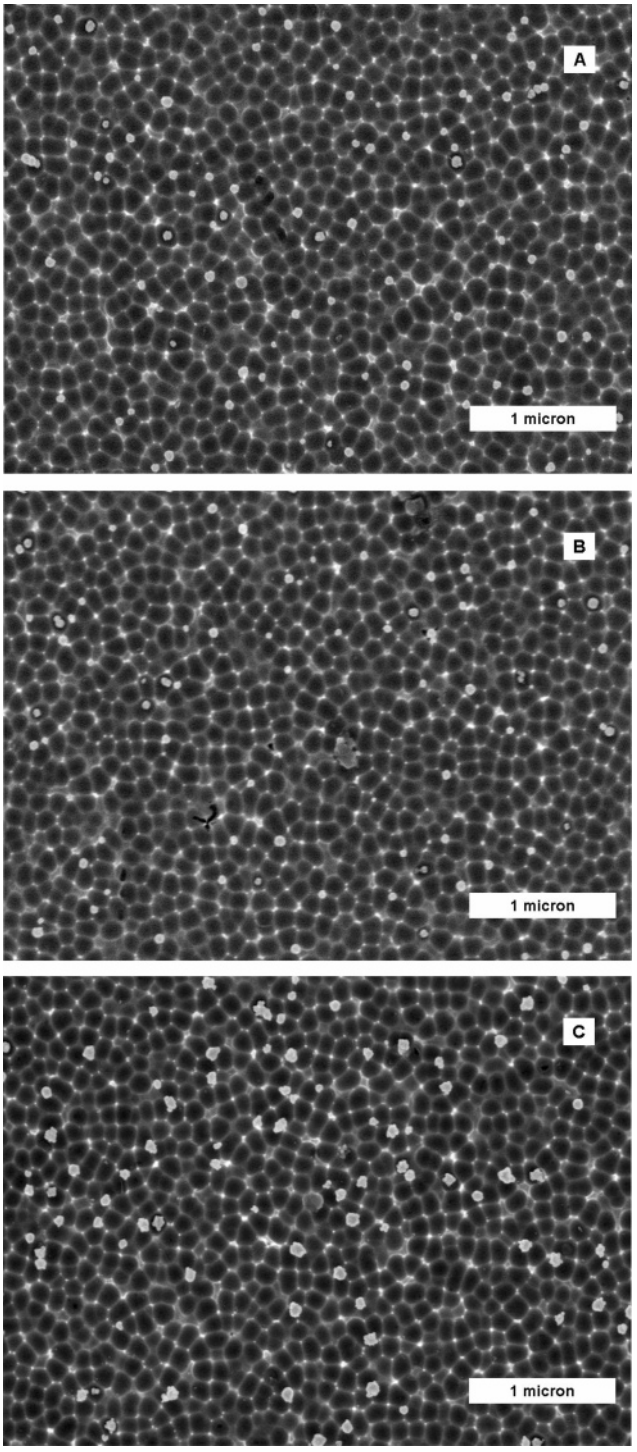


**Figure 2.** SEM micrographs obtained after electrodeposition of gold at −3.95 V vs Ag/AgCl for (A) 0.03, (B) 0.04, and (C) 0.05 s.

$$D = \sqrt[3]{\frac{6QM}{\pi\rho FN}} \quad (1)$$

In eq 1, $M$ is the atomic mass of gold (197 g/mol), $\rho$ is the density of gold ($19 \times 10^6$ $g/m^3$), $F$ is the Faraday constant, and $N$ is the particle coverage ($7 \times 10^8$ particles $cm^{-2}$). The faradaic charge densities, as determined by integrating the faradaic current transients, and calculated particle diameters are shown

**TABLE 1: Mean Particle Diameters and Positions of Absorption Maximum as a Function of Electrodeposition Time**

| electrodeposition time/s | *Q*, faradaic charge density mC cm$^{-2}$ | *D*, particle diameter as *f*(*Q*)/nm | *D*, mean particle diameter by SEM/nm | aspect ratio by SEM | absorption max/nm |
|---|---|---|---|---|---|
| 0.03 | 1.1 | 68 | $42 \pm 12$ | $1.36 \pm 0.36$ | 610 |
| 0.04 | 1.5 | 76 | $49 \pm 12$ | $1.31 \pm 0.25$ | 620 |
| 0.05 | 2.0 | 84 | $74 \pm 17$ | $1.19 \pm 0.13$ | 675 |

in Table 1 (columns 2 and 3). The first method is likely to overestimate the particle diameter because the faradaic efficiency is less than 100%. The more accurate second method is based upon the quantitative analysis of SEM micrographs (Table 1, column 4). As indicated in Table 1, the mean particle diameter increases with the electrodeposition time. Three histograms of particle diameters (Figure 3) corresponding to three micrographs (Figure 2) show that the relative standard deviation of the particle diameter is about 25%. We note that electrodeposition carried out with the same potential and for longer than 0.06 s resulted in a bimodal distribution of particle diameters, with a large population of small particles and a small population of large particles. Similar observations were reported for electrodeposition of gold particles on highly oriented pyrolytic graphite.[46]

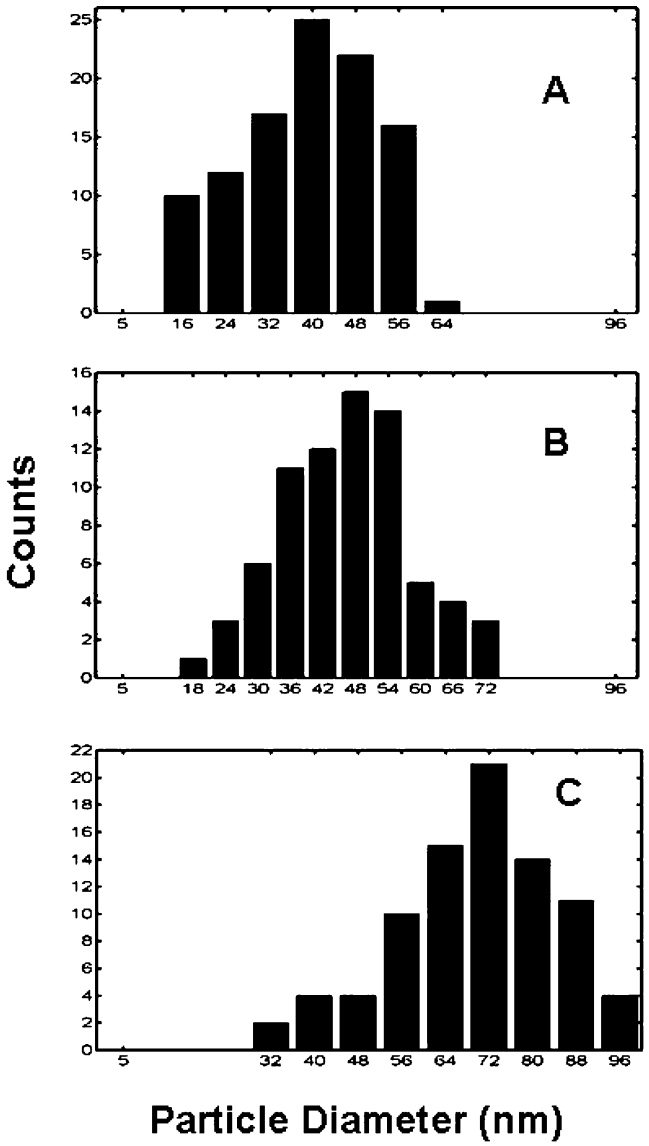


**Figure 3.** Histograms of particle diameters (counts vs particle diameter) corresponding to micrographs shown in Figure 2.

Examination of Figure 2 reveals that there are two preferential sites for electrodeposition of gold particles. Some of the gold particles are located in the middle of scallops. This observation is not surprising since in the middle of scallops the layer of barrier aluminum oxide is likely to be the thinnest. Thus, the electrodeposition current, which exponentially decreases with the thickness of a dielectric layer, becomes "directed" to the middle of scallops. In a similar way, the electroless deposition of silver particles was observed to proceed from the middle of scallops.[42] Unexpected is an observation that gold particles also tend to develop at the top edges of scallops, particularly at those points where three or more individual scallops are adjacent to each other. The physical origin of the second nucleation site needs further investigation. No particles are observed on the slopes of scallops.

Figure 4a,b demonstrates three SE spectra ($\psi$ and $\Delta$) corresponding to three samples represented in Figure 2 (electrodeposition times are 0.03, 0.04, and 0.05 s, respectively). Shown also is a background SE spectrum collected for an anodized and etched aluminum/copper film without gold particles. The experimental data are shown as symbols, and the model-generated data are drawn as solid lines. The SE background spectrum is featureless, as typically observed for

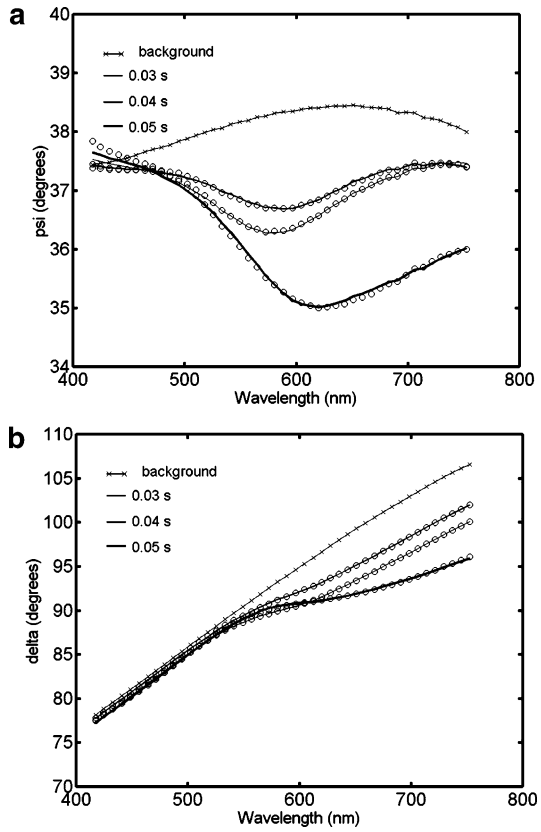


**Figure 4.** Three SE spectra: (a) $\psi$ and (b) $\Delta$ obtained for three samples after electrodeposition for 0.03, 0.04, and 0.05 s. Shown also is a background SE spectrum for an anodized and etched aluminum/copper film (without gold particles). Experimental SE data are symbols and model SE data are solid lines.

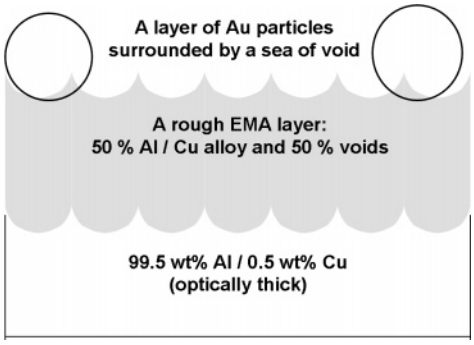


**Figure 5.** Optical model describing gold particles on top of rough and optically thick aluminum/copper substrate.

optically thick metallic films. Comparison of the SE background spectrum and spectra with gold particles indicates that all three $\psi$ sets collected for samples with gold particles demonstrate a depression region around 580−620 nm (Figure 4a). $\psi$ is known to be sensitive to extinction coefficients of deposited films, as opposed to $\Delta$, which is primarily sensitive to the film thickness. As it turns out, the $\psi$ depression region in all three SE spectra corresponds to an absorption peak associated with surface plasmons of gold particles. Moreover, the position of the depression region systematically shifts to higher wavelengths as the mean particle diameter increases from 42 to 74 nm. While the position of the $\psi$ depression regions correlates with the mean particle diameter, the absolute magnitude of the depression peak is likely to be proportional to the coverage of gold particles. Comparison of three $\psi$ depression regions indicates that gold particle coverage for three samples is slightly different. Specifically, the sample with gold particles electrodeposited for 0.04 s shows the smallest decrease in $\psi$ as compared to two other samples. This observation agrees with data obtained from Figure 2b, which indicate this sample had the lowest particle count (Figure 2).

For quantitative analysis of SE spectra, it is necessary to postulate a physically adequate model. The pseudodielectric function of electrodeposited gold mesoparticles is described by using a 50-nm layer consisting of two Lorentz oscillators (eq 2).

$$\epsilon(\lambda) = \epsilon_\infty + \sum_k \frac{A_k}{E_k^2 - \left(\frac{hc}{\lambda}\right)^2 - iB_k\left(\frac{hc}{\lambda}\right)} \qquad (2)$$

In eq 2, $\epsilon_\infty$ is an offset, $h$ is Planck's constant, $c$ is the light speed, and $\lambda$ is the wavelength. For the $k$th oscillator, $A_k$ is the amplitude (oscillator strength), $E_k$ is the center energy, and $B_k$ is the broadening. The model assumed that the particulate film of gold had a constant thickness of 50 nm, because of a strong correlation between film thickness and oscillator strengths. The complete two-layer optical model (Figure 5) describing gold particles on a rough aluminum/copper substrate includes the layer with two Lorentz oscillators, the 50-nm thick Bruggeman EMA layer (as described in the Experimental Section), and the optically thick aluminum/copper substrate. The model does not include a layer of barrier aluminum oxide because it is optically thin (1.5 nm). Table 2 summarizes the six model parameters obtained by fitting the acquired SE data to the postulated model for each of three samples (electrodeposition times of 0.3, 0.4, and 0.5 s). Shown also is the mean-squared error (MSE), which is defined as a sum of the squares of the differences between measured and calculated data, with each difference weighted by the standard deviation of that measured data point.

**TABLE 2: Results of Modeling of SE Data**

| | electrodeposition time/s | | |
|---|---|---|---|
| parameter | 0.03 | 0.04 | 0.05 |
| $A_1$ | 0.13 ± 0.02 | 0.084 ± 0.013 | 0.091 ± 0.04 |
| $B_1$ | 0.62 ± 0.02 | 0.65 ± 0.03 | 0.58 ± 0.06 |
| $E_1$/eV | 2.085 ± 0.016 | 2.054 ± 0.007 | 2.002 ± 0.028 |
| $A_2$ | 0.047 ± 0.022 | 0.031 ± 0.015 | 0.12 ± 0.04 |
| $B_2$ | 0.63 ± 0.10 | 0.97 ± 0.14 | 0.67 ± 0.09 |
| $E_2$/eV | 1.81 ± 0.06 | 1.70 ± 0.10 | 1.73 ± 0.05 |
| MSE | 0.99 | 0.62 | 1.74 |

Both closely positioned Lorentz oscillators (∼2.05 and ∼1.75 eV) are likely to represent the light absorption of gold particles associated with surface plasmons. In contrast to a single Lorentz oscillator used elsewhere,[35,36] our model requires two Lorentz oscillators to describe surface plasmon absorption. The need for two oscillators may be due to the shape of deposited gold particles, which are not perfectly spherical. As indicated in Table 1, the aspect ratios are approximately 1.3. Metallic particles with the aspect ratio of approximately 3 have been previously shown to have two distinct surface plasmon bands separated by about 250 nm (0.77 eV).[4] In addition, slight polydispersity in particle diameters for a given sample may also require using the second Lorentz oscillator.

The optical constants of gold particles ($n$ and $k$) are calculated (Figure 6) by using six fitting parameters of two Lorentz oscillators for each of three samples. As indicated above, three samples had slightly different coverage of gold particles. However, in the modeling of SE data all three samples are assumed to have the same coverage and, correspondingly, the same thickness of the layer with two Lorentz oscillators. As a result, magnitudes of calculated optical constants are coupled

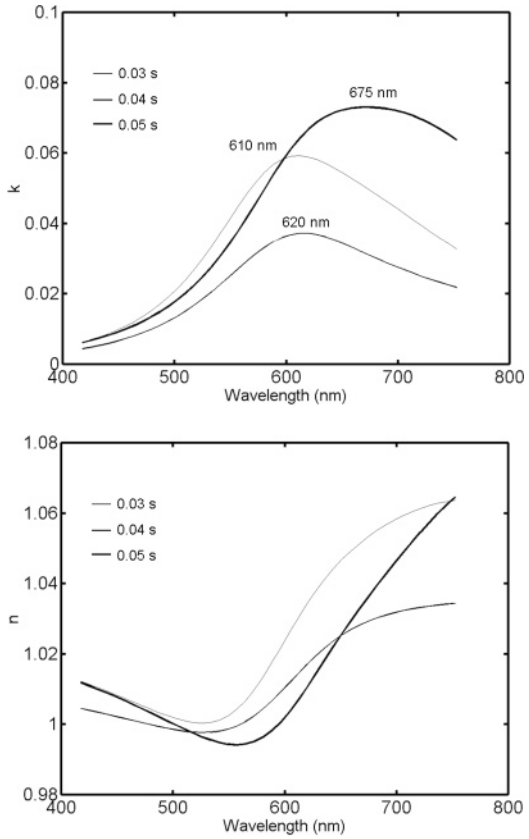


**Figure 6.** Three sets of calculated optical constants of gold particles: (a) extinction coefficient, $k$, and (b) refractive index, $n$. Gold particles were obtained after electrodeposition for 0.03, 0.04, and 0.05 s.

to the actual particle coverage. This point is illustrated by noting that the largest deviation of $\psi$ (electrodeposition time of 0.05 s) from the background signal (Figure 4a) corresponds to the largest magnitude of $k$ (Figure 6a). Regardless of the coupling between the particle coverage and magnitude of optical constants, the particle coverage is not expected to influence the position of absorption bands. This assumption can be justified by examining Figure 2, which indicates that on average gold particles are located sufficiently far away from each other. Therefore, their optical constants are not affected by the presence of the neighboring particles.

Analysis of Figure 6a results in three conclusions. First, the position of absorption maximum, as indicated by labels (Figure 6a), shifts to longer wavelengths as the mean particle diameter increases (Table 1). This trend is consistent with previously reported results. In the extrinsic size region (the diameter of gold particles is more than 25 nm), absorption maximums are red shifted with increasing particle diameter.[4,5,25,26] Second, in comparison with gold particles of the same size (50−70 nm) in solution, electrodeposited gold particles have absorption bands shifted about 80−100 nm to longer wavelengths. This shift is most likely due to the fact the gold particles are deposited on an aluminum/copper substrate. The dielectric constant of a substrate is known to affect the positions of absorption bands. For example, the extinction maximum of localized surface plasmons of silver nanoparticles was shown to shift to longer wavelengths with increasing refractive index of the substrate.[47] Our SE results at 620 nm show that the optical constants of anodized and etched aluminum/copper substrate are $n = 1.1$ and $k = 6.1$. Thus, the substrate may be responsible for the observed red shift of absorption maximums. Third, our SE measurements do not allow us to establish whether there is any increase in the bandwidth of the surface plasmon absorption band with an increase in the mean particle diameter as observed in the extrinsic size region.[4] This fact may be explained by the coupling of the calculated optical constants to the coverage of gold particles.

In addition to the analysis of extinction coefficients, it would be interesting to examine refractive indexes of deposited particulate films (Figure 6b). Under our electrodeposition conditions, gold particles occupy only a small volume fraction on the substrate surface (Figure 2). Our optical model describes the gold particles as a continuous planar layer. This layer consists of widely distributed gold particle inclusions imbedded in a sea of void. Thus, refractive indexes of particulate gold films are very close to that of air ($n \sim 1.02$ at 633 nm). The previously reported refractive indexes of nanocomposite gold films were significantly higher ($\sim$1.6)[35,36] due to the employment of organic molecules to immobilize gold particles on a substrate.

Combined analysis of optical constants, $k$ and $n$, allows us to conclude that electrodeposition on aluminum/copper films results in the formation of gold mesoparticles, which show an optical response measurable by SE. Moreover, the absorption maximum shifts to longer wavelengths as the mean particle diameter increases. Therefore, electrodeposition is demonstrated to be a facile method to fabricate particulate films with distinct optical properties. To our knowledge, electrodeposition has not been previously shown to produce gold particles on a substrate under conditions which enable their absorption bands due to surface plasmons to be resolved. The optical properties of electrodeposited gold particles can be exploited in a variety of electronic, optical devices and biosensors.[48] Moreover, the procedure for electrodeposition on aluminum/copper films can be extended in order to deposit other metallic particles (e.g. Cu, Cd), which subsequently can be transformed to semiconductor salts by chemical oxidation and displacement reactions.[49] Thus, this method represents an opportunity to fabricate semiconductor particles on technologically relevant substrates.

## Conclusions

Electrodeposition of gold mesoparticles on anodized and chemically etched aluminum/copper films provides a facile and inexpensive method to achieve the 2D arrangement of metallic particles on a technologically important substrate. Under the reported experimental conditions, electrodeposition of gold particles occurs by instantaneous nucleation and with no diffusion limitations. Taking advantage of these two characteristics of the electrodeposition process, gold particles are electrodeposited with the particle coverage of $7 \times 10^8$ particles $cm^{-2}$, the mean particle diameter in the range of 40−80 nm, and the relative standard deviation of the particle diameter of 25%. The optical constants of gold mesoparticles electrodeposited on optically thick aluminum/copper films are determined by SE. The absorption peak, associated with surface plasmons, shifts from 610 to 675 nm as the mean particle diameter increases from 42 to 74 nm. Refractive indexes of particulate gold films are very close to that of air ($n \sim 1.02$ at 633 nm). Electrodeposition of gold particles with a narrow distribution of particle diameters on aluminum/copper films is expected to increase the utility of gold particles and facilitate their incorporation in nanostructured materials and devices.

**Acknowledgment.** This work was supported in part by the Center for Micro-Engineered Materials (UNM). The SEM laboratory was supported by the New Mexico EPCoR NSF grant and the NNIN grant. We thank Todd M. Bauer (Sandia National Laboratories, Albuquerque, NM) for fabrication of silicon wafers with an aluminum/copper layer, Tim S. Olson (UNM) for quantitative analysis of micrographs, and Prof. Gabriel P. Lopez (UNM) for critical reading of this paper.

## References and Notes

(1) Bradley, J. S.; Schmid, G. In *Nanoparticles*: *From Theory to Application*; Schmid, G., Ed.; Wiley-VCH, Weinheim, Germany, 2004; p 186.
(2) Goia, D. V. *J. Mater. Chem.* **2004**, *14*, 451.
(3) Daniel, M. C.; Astruc, D. *Chem. Rev.* **2004**, *104*, 293.
(4) Link, S.; El-Sayed, M. A. *J. Phys. Chem. B* **1999**, *103*, 8410.
(5) El-Sayed, M. A. *Acc. Chem. Res.* **2001**, *34*, 257.
(6) Shipway, A. N.; Katz, E.; Willner, I. *ChemPhysChem* **2000**, *1*, 18.
(7) Corti, C. W.; Holliday, R. J.; Thompson, D. T. *Gold Bull.* **2002**, *35*, 111.
(8) Hutter, E.; Fendler, J. H. *Adv. Mater.* (*Weinheim, Ger.*) **2004**, *16*, 1685.
(9) Xia, Y.; Halas, N. J. *MRS Bull.* **2005**, *30*, 338.
(10) Oskam, G.; Long, J. G.; Natarajan, A.; Searson, P. C. *J. Phys. D*: *Appl. Phys.* **1998**, *31*, 1927.
(11) Budevski, E.; Staikov, G.; Lorenz, W. J. *Electrochim. Acta* **2000**, *45*, 2559.
(12) Penner, R. M. *J. Phys. Chem. B* **2002**, *106*, 3339.
(13) Oskam, G.; Searson, P. C. *J. Electrochem. Soc.* **2000**, *147*, 2199.
(14) Krumm, R.; Guel, B.; Schmitz, C.; Staikov, G. *Electrochim. Acta* **2000**, *45*, 3255.
(15) Ji, C. X.; Oskam, G.; Searson, P. C. *J. Electrochem. Soc.* **2001**, *148*, C746.
(16) Radisic, A.; Cao, Y.; Taephaisitphongse, P.; West, A. C.; Searson, P. C. *J. Electrochem. Soc.* **2003**, *150*, C362.
(17) Radisic, A.; Oskam, G.; Searson, P. C. *J. Electrochem. Soc.* **2004**, *151*, C369.
(18) Zoval, J. V.; Stiger, R. M.; Biernacki, P. R.; Penner, R. M. *J. Phys. Chem.* **1996**, *100*, 837.
(19) Zoval, J. V.; Lee, J.; Gorer, S.; Penner, R. M. *J. Phys. Chem. B* **1998**, *102*, 1166.

(20) Stiger, R. M.; Gorer, S.; Craft, B.; Penner, R. M. *Langmuir* **1999**, *15*, 790.
(21) Marquez, K.; Staikov, G.; Schultze, J. W. *Trans. Inst. Met. Finish*. **2002**, *80*, 73.
(22) Ziegler, J. C.; Reitzle, A.; Bunk, O.; Zegenhagen, J.; Kolb, D. M. *Electrochim. Acta* **2000**, *45*, 4599.
(23) Radisic, A.; Oskam, G.; Searson, P. C. *J. Electrochem. Soc*. **2004**, *151*, C369.
(24) Hsiao, G. S.; Anderson, M. G.; Gorer, S.; Harris, D.; Penner, R. M. *J. Am. Chem. Soc.* **1997**, *119*, 1439.
(25) Kreibig, U.; Vollmer, M. *Optical Properties of Metal Clusters*; Springer-Verlag: Berlin, Germany, 1995; p 13.
(26) Link, S.; El-Sayed, M. A. *Int. Rev. Phys. Chem*. **2000**, *19*, 409.
(27) Hilger, A.; Tenfelde, M.; Kreibig, U. *Appl. Phys. B* **2001**, *73*, 361.
(28) Mulvaney, P. *Langmuir* **1996**, *12*, 788.
(29) Link, S.; El-Sayed, M. A. *J. Phys. Chem. B* **1999**, *103*, 4212.
(30) Jensen, T. R.; Malinsky, M. D.; Haynes, C. H.; Van Duyne, R. P. *J. Phys. Chem. B* **2000**, *104*, 10549.
(31) Greef, R. *Thin Solid Films* **1993**, *233*, 32.
(32) Suni, I. I. *J. Appl. Electrochem.* **1997**, *27*, 1219.
(33) Urban, F. K.; Hosseini-Tehrani, A.; Khabari, A.; Griffiths, P.; Bungay, C.; Petrov, I.; Kim, Y. *Thin Solid Films* **2002**, *408*, 211.
(34) Kooij, E. S.; Wormeester, H.; Brouwer, E. A. M.; van Vroonhoven, E.; van Silfhout, A.; Poelsema, B. *Langmuir* **2002**, *18*, 4401.
(35) Zhang, H.-L.; Evans, S. D.; Henderson, J. R. *Adv. Mater*. **2003**, *15*, 531.
(36) Cant, N. E.; Zhang, H.-L.; Critchley, K.; Mykhalyk, T. A.; Davies, G. R.; Evans, S. D. *J. Phys. Chem. B* **2003**, *107*, 13557.
(37) Joerger, R.; Gampp, R.; Heinzel, A.; Graf, W.; Kohl, M.; Gantenbein, P.; Oelhafen, P. *Sol. Energy Mater. Sol. Cells* **1998**, *54*, 351.
(38) Dalacu, D.; Martinu, L. *J. Appl. Phys*. **2000**, *87*, 228.
(39) Girardeau, T.; Camelio, S.; Babonneau, D.; Toudert, J.; Barrranco, A. *Thin Solid Films* **2004**, *455*−*456*, 313.
(40) Olson, T. S.; Atanassov, P.; Brevnov, D. A. *J. Phys. Chem. B* **2005**, *109*, 1243.
(41) Green, T. A.; Liew, M.-J.; Roy, S. *J. Electrochem. Soc*. **2003**, *150*, C104.
(42) Brevnov, D. A.; Olson, T. S.; Lopez, G. P.; Atanassov, P. *J. Phys. Chem. B* **2004**, *108*, 17531.
(43) Strehblow, H. H.; Melliar-Smith, C. M.; Augustyniak, W. M. *J. Electrochem. Soc.* **1978**, *125*, 915.
(44) Habazaki, H.; Zhou, X.; Shimizu, K.; Skeldon, P.; Thompson, G. E.; Wood, G. G. *Electrochim. Acta* **1997**, *42*, 2627.
(45) Paez, M. A.; Bustos, O.; Thompson, G. E.; Skeldon, P.; Shimizu, K.; Wood, G. C. *J. Electrochem. Soc.* **2000**, *147*, 1015.
(46) Boxley, C. J.; White, H. S.; Lister, T. E.; Pinhero, P. J. *J. Phys. Chem. B* **2003**, *107*, 451.
(47) Malinsky, M. D.; Kelly, K. L.; Schatz, G. C.; Van Duyne, R. P. *J. Phys. Chem. B* **2001**, *105*, 2343.
(48) Haes, A. J.; Zou, S.; Schatz, G. C.; Van Duyne, R. P. *J. Phys. Chem. B* **2004**, *108*, 6961.
(49) Penner, R. M. *Acc. Chem. Res.* **2000**, *33*, 78.